catalysts

MDPI

Article

CO_2 Electroreduction by Engineering the Cu_2O/RGO Interphase

Matteo Bisetto [1,2,*], Sourav Rej [3], Alberto Naldoni [4], Tiziano Montini [1,5], Manuela Bevilacqua [5,6,*] and Paolo Fornasiero [1,2,5]

1 Department of Chemical and Pharmaceutical Sciences, University of Trieste, Via L. Giorgieri 1, 34127 Trieste, Italy
2 National Interuniversity Consortium of Materials Science and Technology (INSTM), University of Trieste, Via L. Giorgieri 1, 34127 Trieste, Italy
3 Czech Advanced Technology and Research Institute, Regional Centre of Advanced Technologies and Materials (RCPTM), Palacký University Olomouc, Šlechtitelů 27, 77900 Olomouc, Czech Republic
4 Department of Chemistry and NIS Centre, University of Turin, Via P. Giuria 7, 10125 Turin, Italy
5 Institute of Chemistry of Organometallic Compounds (ICCOM), National Research Council (CNR), Trieste Research Unit, University of Trieste, Via L. Giorgieri 1, 34127 Trieste, Italy
6 Institute of Chemistry of Organometallic Compounds (ICCOM), National Research Council (CNR), Via Madonna del Piano 10, 50019 Sesto Fiorentino, Italy
* Correspondence: mbisetto@instm.it (M.B.); manuela.bevilacqua@iccom.cnr.it (M.B.)

Abstract: In the present investigation, Cu_2O-based composites were successfully prepared through a multistep method where cubic Cu_2O nanoparticles (CU Cu_2O) have been grown on Reduced Graphene Oxide (RGO) nanosheets. The structural and morphological properties of the materials have been studied through a comprehensive characterization, confirming the coexistence of crystalline Cu_2O and RGO. Microscopical imaging revealed the intimate contact between the two materials, affecting the size and the distribution of Cu_2O nanoparticles on the support. The features of the improved morphology strongly affected the electrochemical behavior of the composites, increasing the activity and the faradaic efficiencies towards the electrochemical CO_2 reduction reaction process. CU Cu_2O/RGO 2:1 composite displayed selective CO formation over H_2, with higher currents compared to pristine Cu_2O (-0.34 mA/cm^2 for Cu_2O and -0.64 mA/cm^2 for CU Cu_2O/RGO 2:1 at the voltage of -0.8 vs. RHE and in a CO_2 atmosphere) and a faradaic efficiency of 50% at -0.9 V vs. RHE. This composition exhibited significantly higher CO production compared to the pristine materials, indicating a favorable *CO intermediate pathway even at lower voltages. The systematic investigation on the effects of nanostructuration on composition, morphology and catalytic behavior is a valuable solution for the formation of effective interphases for the promotion of catalytic properties providing crucial insights for future catalysts design and applications.

Keywords: electrochemical CO_2 reduction reaction; nanostructured Cu_2O; Cu_2O/RGO interphase; CO production

Citation: Bisetto, M.; Rej, S.; Naldoni, A.; Montini, T.; Bevilacqua, M.; Fornasiero, P. CO_2 Electroreduction by Engineering the Cu_2O/RGO Interphase. *Catalysts* **2024**, *14*, 412. https://doi.org/10.3390/catal14070412

Academic Editor: Carlo Santoro

Received: 24 May 2024
Revised: 20 June 2024
Accepted: 21 June 2024
Published: 28 June 2024

1. Introduction

The significant increase in CO_2 greenhouse gas and the care about the security of energy supply have received great interest and are considered as the main challenges of our century. In particular, the conversion of CO_2 into useful chemicals, building blocks, energy vectors and/or fuels by photochemistry and electrocatalysis have been considered as one of the most advanced approaches to limit both energy and environmental problems at the same time [1–3]. Many promising and low-cost photo/electrocatalysts, non-precious metal-based or metal-free composite materials have been documented in the more recent literature; otherwise the design of adequate candidate composite electrocatalysts in terms of efficiency and selectivity needs to be also related to the critical impact of the adopted synthesis pathway [4–9].

In the last three decades, copper oxides, particularly Cu_2O, have been considered as important precursors for preparing Cu-based catalysts for electrochemical CO_2 reduction reaction (CO_2RR), due to the improved electrocatalytic performance compared to untreated metallic Cu [10,11]. In the study presented by D. Ren et al. in 2015, metallic Cu exhibited a Faradaic Efficiency (FE) of 13.8% for ethylene (C_2H_4) and 0% for ethanol (C_2H_5OH) at −1.0 V vs. RHE. In contrast, under the same conditions the equivalent oxide-derived Cu film catalyst achieved an optimized FE of ca. 39% and ca. 16% for C_2H_4 and C_2H_5OH, respectively, mainly dependent on the specific film thickness [12]. Although copper oxides (CuO and Cu_2O) are generally fast reduced to metallic Cu under CO_2RR conditions according to the Pourbaix diagram, there are other factors that can be discussed to rationalize the relationship between the activity, the selectivity and stability of oxide-derived Cu catalysts, including morphological modifications, defect creation, local pH changes, etc. [13,14].

Cu-based nanostructures characterized by cubic morphology have showed an increased selectivity toward the desired C_{2+} reaction products, and are considered a point of reference in the state of the art [15–19]. In fact, it has been proved that specific morphological parameters of cubic NPs, in particular the size and the surface properties, could be responsible for better control of the selectivity and stability [20,21]. On the other hand, it is not completely clear which parameter of the synthesis could be strongly responsible for a particular obtained morphology: the comprehension of this aspect is fundamental to fine-tune the NPs structure and consequently to optimize their electrocatalytic properties [22]. Importantly, the addition of a carbon-based support to well disperse the cubic Cu_2O (CU Cu_2O) NPs and/or to induce a synergic behavior due to the presence on multiple and different interacting active sites has to be taken into account in order to enhance the interphase role [23–25]. Very recently, Ze-lin Wu et al. published a review work focused on the use of graphene-based support material for CO_2RR electrocatalysts [26]. In this context, graphene is considered an attractive carbon material due to the particular two-dimensional structure, combined with the high specific surface area, a good chemical and mechanical stability and a facile tunability for anchoring different second phase compounds through physical and chemical coupling interactions [27,28]. For these multiple advantages, graphene has been widely explored as either the catalytically active material or the supporting platform in the construction of advanced CO_2RR electrocatalysts. The Reduced Graphene Oxide differs from the precursor Graphene Oxide (GO) in terms of morphology, optical and electrical properties [29,30]. In 2017 E. Jaafar and co-workers highlighted that a folded and wrinkled structure has been observed for RGO with respect to GO [31]. This folding structure can be found on both surface and the edge of RGO due to the losses of oxygen functional groups. Furthermore, they observed that a more folded and wrinkled structure could be produced when the reduction was stressed. By the point of view of electrical behavior, the total current registered for a thin film of RGO deposited on a common glassy carbon support was higher when compared to a similar texture of GO. Once again, this feature was attributed to an oxygen decrease in reduced graphene oxide. In the present work we prepared different composites based on cubic Cu_2O/RGO and we have used them as electrocatalysts towards the CO_2RR. Different efforts have been spent to characterize the obtained materials, with the aim to examine the intrinsic effects of the coupling between the two counterparts of the heterostructure. We deepened the relationship between the morphological, structural and electric properties of CU Cu_2O/RGO composites and the corresponding performance evaluated for CO_2RR, to identify the keys for tuning their electrochemical activity and selectivity. Remarkably, catalytic experiments revealed an improved selectivity towards the formation of CO, demonstrating the potential of the proposed material for applications focused on CO_2 conversion.

2. Results and Discussion

2.1. Characterization of CU Cu_2O/RGO Composites

CU Cu_2O/RGO composites were prepared by growing cubic nanoparticles of Cu_2O directly on the sheets of RGO (Figure 1). RGO was firstly obtained via a two-step process

where graphite was exfoliated and oxidized to form nanosheets of GO through a modified Hummer's method and later partially reduced by addition of hydrazine on the solution to form RGO nanosheets. Cubic Cu_2O nanoparticles were directly grown on the support, using different fractions of RGO. The different amount of RGO affects the stability of the composite and its catalytic behavior, with lower affinity between the two counterparts with a higher fraction of support. For this reason, three different compositions had been selected (CU Cu_2O/RGO 2:1, 1:1 and 1:2) in order to understand the effects of the interaction between the two counterparts of the composite towards the overall catalytic behavior.

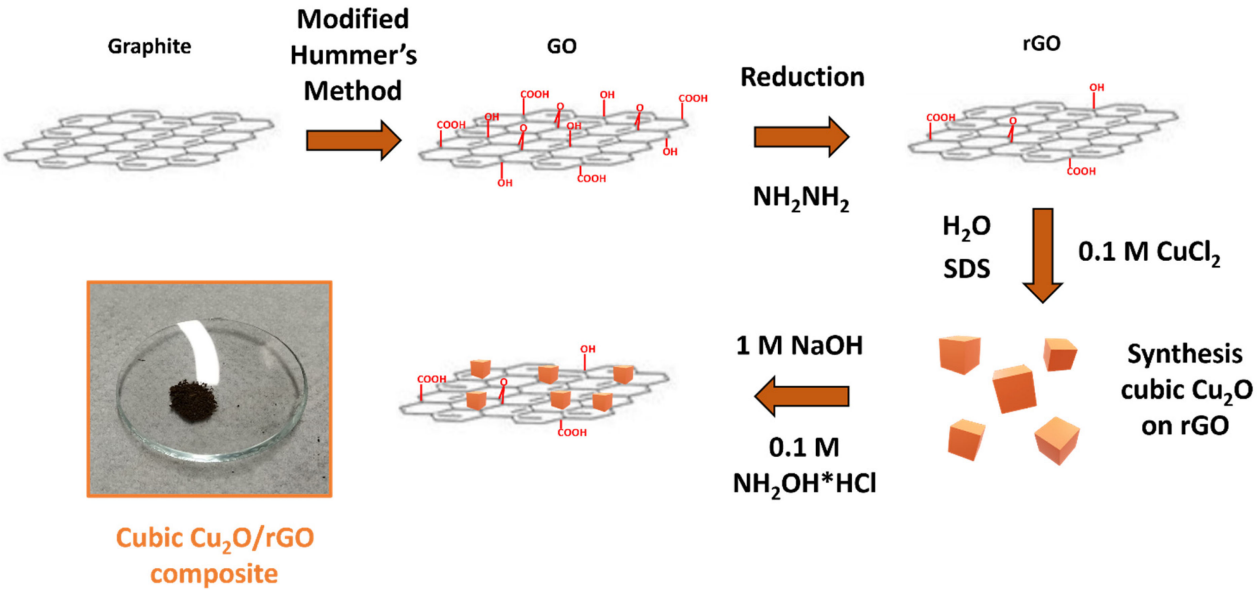

Figure 1. Experimental procedure for the synthesis of cubic Cu_2O/RGO electrocatalysts.

The crystalline structure of the as-prepared catalyst was revealed by XRD. The synthesis allowed the formation of crystalline Cu_2O nanoparticles, with all the typical feature of Cu_2O revealed by XRD diffractograms (Figure 2a) [32]. The chemical stability of the nanoparticles was confirmed by the absence of any reflection related to metallic Cu or CuO. Moreover, the Rietveld analysis allowed quantitative information regarding the crystalline structure of Cu_2O to be obtained, which showed a lattice parameter of 4.27 Å, in good agreement with previously reported values (Figure S1) [33]. No shifts of the position for Cu_2O reflections were detected, suggesting that the introduction of RGO has negligible effects on the crystalline structure of the pristine Cu_2O [34]. Raman spectra of the composites (Figure 2b) confirmed the contemporaneous presence of Cu_2O and RGO by revealing the characteristic vibrations of both phases [35,36]. From the analysis of the fingerprint, it is possible to observe the typical vibrations of Cu_2O and discriminate them from those of CuO, supporting the purity of the chemical phase observed from XRD. The characteristic features of RGO were identified by the typical D-band observed at 1340 cm^{-1} related to the breathing mode of phonons of A_{1g} symmetry while the G-band at 1592 cm^{-1} arises from the first-order scattering of E_{2g} phonons by sp^2 carbon of GO [37,38]. D-band and G-band are observed also in the pristine RGO (Figure S2) discriminating RGO from GO; indeed, the higher intensity of the D-band peak can be related to the removal of oxygen moieties from GO after reduction and suggested the presence of RGO instead of GO [39,40]. The different intensities between the two families of peaks are indicative of the relative composition for the prepared materials.

TGA measurements performed up to 800 °C in air allowed to understand the thermal stability of the different materials with the variation of the temperature (Figure 2c). The mass of the material decreased in the first part of the thermal treatment due to the desorption of the adsorbed water molecules while the rapid reduction of the mass around 400–500 °C is characteristic of CO and CO_2 pyrolysis on graphene-like materials [29,41].

The thermal treatment in air had implications even on the Cu_2O material, with a conversion to CuO through the reaction $2Cu_2O + O_2 \rightarrow 4CuO$ [42]. From the analysis of the reported trends, it is possible to calculate the fraction of initial Cu_2O on the prepared composites, revealing an experimental fraction of Cu_2O similar to the theoretical just in the composite 2:1 and confirming the improved affinity of the two materials in the latter case compared to the other composites (Table S1).

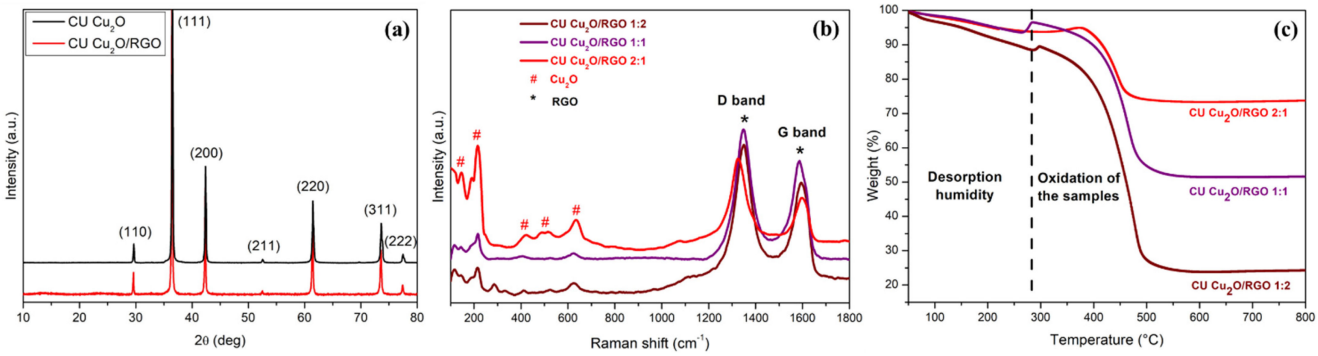

Figure 2. (**a**) XRD patterns for pristine nanoparticles of Cu_2O and for the composite with RGO. (**b**) Raman spectra for the different synthetized composites where it is possible to observe the characteristic vibrations of Cu_2O (#) and RGO (*). (**c**) Thermal Gravimetric Analysis for the three different composites in air with the temperature range 50–800 °C.

SEM and TEM images revealed that the obtained pristine RGO is characterized by thin and crumpled sheets, with different platelets closely associated with each other (Figure S3). The synthesis of unsupported Cu_2O nanoparticles allowed the formation of cubes bounded with six (100) facets and an average dimension of 200 nm (±20 nm) (Figures S3 and S4a). When the synthesis of Cu_2O occurred in a dispersion of RGO, the cubic Cu_2O nanoparticles were directly grown on the support, thanks to the stabilizing features of RGO sheets (Figure 3). TEM images confirmed the intimate contact between the two materials of the catalyst, with the nanostructures that are fully bounded by the 3D plates of RGO (Figure 3a,b). On the other hand, the formation of the composites altered the dimension of Cu_2O nanoparticles, with an average size of 150 nm for Cu_2O/RGO 2:1, slightly decrease than the unsupported material (Figure 3c,d). The other compositions showed comparable average sizes, intermediate between the pristine and the supported materials (Figure S4 and Table S2). The formation of the proper composite is demonstrated even through EDX, confirming the presence of characteristics elements such as Cu or O and revealing high percentage of C-species due to the RGO support (Figure 3e).

2.2. Electrochemical Behavior of CU Cu_2O/RGO Composites and CO_2RR Tests

The electrocatalytic behavior of the different materials was firstly characterized using the typical three-electrode setup, depositing an ink of the specific material on the surface of a Rotating Disc Electrode (RDE, Figures S5 and S6). The presented Linear Sweep Voltammetries (LSVs) and ChronoAmperometries (CAs) showed a different behavior under the Ar and CO_2 atmosphere, indicating a dependency of the activity from the atmosphere and an overall influence on the catalytic pathway of the electrocatalysts. The formation of the composites has implications on the overall activity of Cu_2O, with higher current of the Cu_2O/RGO system due to the improved dispersion of Cu_2O cubes and the intimate contact within the sheets of RGO (i.e., -0.34 mA/cm^2 for Cu_2O and -0.64 mA/cm^2 for CU Cu_2O/RGO 2:1 at the voltage of -0.8 V vs. RHE in the CO_2 atmosphere; this feature can be observed for all the other composites). The reduction peak of Cu_2O to metal Cu is observed at -0.2 V vs. RHE, showing a modification of the material due to the application of the negative voltage. Concerning the stability of the catalyst, no decays or rapid changes of the currents were observed during the chronoamperometric tests; otherwise, a general decrease in the current was observed after a few minutes from the application of the voltage followed

by a stable response for the 90 min of electrochemical characterization. The decreasing of the current is related to the rapid reduction of the Cu(I) phase to metallic copper under the application of a constant voltage and the subsequent stabilization of the phase during the first minutes of the analysis [43]. Moreover, according to the Electrochemical Impedance Spectroscopy (EIS) data summarized in the Nyquist plot of Figure S7, the total impedance strongly decreases for the composite materials with respect to both the pristine CU Cu_2O and the carbon RGO support, accounting for enhanced charge transfer and diffusive contributes; furthermore, in the range of ca. 1–5 kHz frequencies, Z values referred to the coupled electrocatalysts are still lower than the separate phases, suggesting an improved charge transfer that could be mediated by the intimate contact of Cu and RGO (Figure S7b).

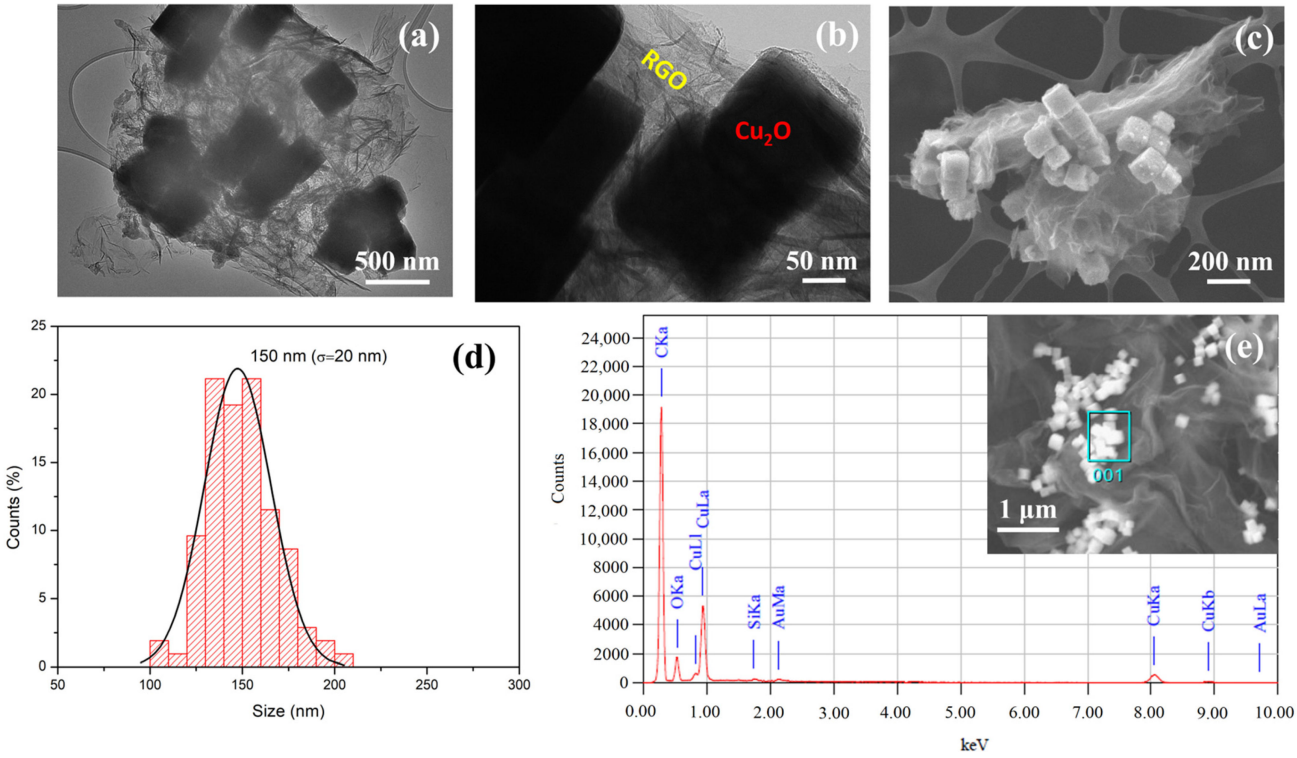

Figure 3. Microscope analysis for the composite Cu_2O/RGO 2:1. (**a**,**b**) TEM images at different magnification levels. (**c**) SEM image of the cubic nanoparticles of Cu_2O growth on RGO surface. (**d**) Size distribution of Cu_2O nanoparticles (count: 400 nanoparticles). (**e**) EDX image and elemental distribution for the considered composite.

An in-deep electrochemical CO_2RR characterization had been performed to unveil the role of CO_2 on different catalysts behavior, analyzing the performances of the materials in terms of current and productivity. Chronoamperometries at different voltages (−0.7 V, −0.9 V and −1.1 V vs. RHE) were used to evaluate the dependency of the activity from the applied potential. The detailed characterization at the voltage of −0.9 V is presented in Figure 4 while the other voltages are reported in the supporting information (Figures S8 and S9). Compared to the pristine materials, all the composites showed an improved current density especially at lower potentials (i.e., −1.79 mA/cm^2 for Cu_2O and −2.72 mA/cm^2 for CU Cu_2O/RGO 2:1 at the voltage of −0.9 V vs. RHE in the CO_2 atmosphere), evidencing that the higher exposed area of the materials and the intrinsic affinity between the two counterparts affected the overall electrochemical response in a beneficial way (Figure 4a). The different products from the catalytic process were tracked using gas and liquid chromatography, analyzing the overall quantities and calculating the relative total FEs at the proper potential for the 120 min of characterization.

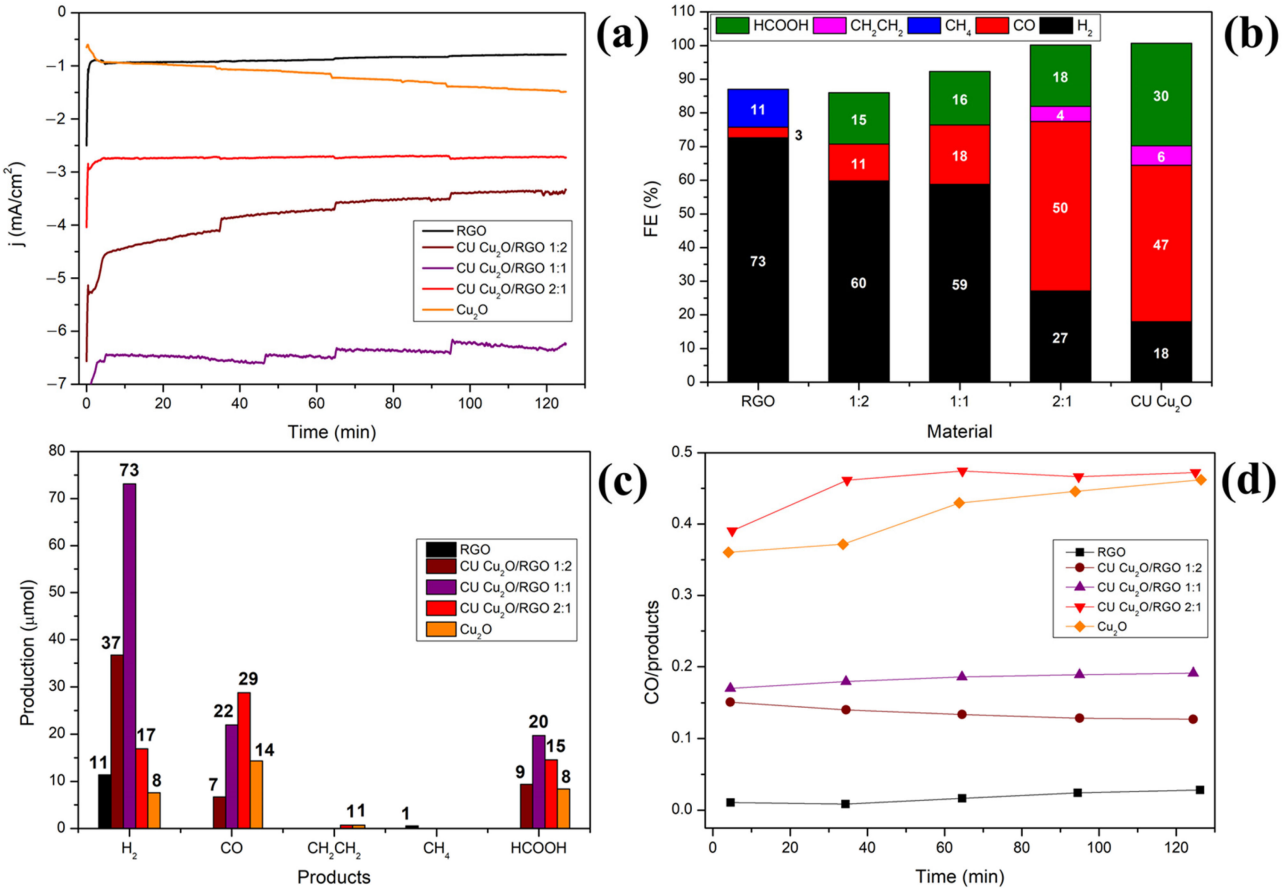

Figure 4. CO_2RR tests for the different composites of CU Cu_2O/RGO at the voltage of −0.9 V vs. RHE. (**a**) Two hour chronoamperometries under saturated CO_2 atmosphere. (**b**) FEs of gaseous and liquid products. (**c**) Products distribution (μmol) of the different compounds after 2 h chronoamperometries. (**d**) Production profile of CO during the experiment for the different composite materials.

The improved electrochemical phase boundary of the CU Cu_2O/RGO texture increased the current of the materials, and it had implications on the selectivity and productivity, limiting the formation of H_2 and shifting the activity towards the CO_2RR. Moreover, for the quasi-total reactivity of bare RGO toward the HER process [44], the different composites showed higher faradaic efficiencies for the formation of CO_2RR products, in particular CO and $HCOO^-$ (Figure 4b). Among the different catalytic pathways, CO_2 can be reduced forming CO or formic acid, depending on which part of the CO_2 molecule interacts with the surface of the catalyst [45]. As it was reported, 100-like Cu domains are able to trigger the formation of C-C bond and selectively induce the production of *CO species [46]. Therefore, the addition of cubic Cu_2O has implications on the overall behavior of RGO, leading to the adsorption of CO_2 molecules via a $*CO_2$ intermediate and explaining a favorable CO formation compared to the other products [47]. As a result of the different catalytic responses of the composites, the FE_{H_2} dropped from 73% for the pristine RGO to 18% for the unsupported CU Cu_2O, and a contemporaneous improving of the selectivity for the CO formation is observed, with the composite CU Cu_2O/RGO 2:1 characterized by a FE_{CO} of 50%, the highest FE_{CO} between all the materials. The material showed also a FE_{HCOO^-} of 18%, higher than the other prepared composites. Formic acid is considered an interesting hydrogen storage thanks to the high energy density and the fact that, being a liquid product, it can be separated easily from the rest of the other products of catalysis [48]. In this optic, the comparison of FE_{HCOO^-} for the different materials allows confirmation of the beneficial interaction between the two counterparts of the composite. The obtained selectivity, coupled with the increased current of the composite, provided a higher amount of CO during the experiments, more than double compared with unsupported Cu_2O (29 μmol

vs. 14 µmol, respectively) and suggested a favored pathway toward the formation of CO (Figure 4c). The high fraction of RGO in the composites 1:1 and 1:2 still has implication on the overall H_2 selectivity, with an approximately FE_{H_2} of 60%, and productivity, affected also by the higher current. The analysis of the ratio between the moles of CO and the moles of all the products quantified during the CA test for these specified compositions showed a decrease in the ratio due to the increased selectivity toward HER and a correlation with the increasing of RGO content (Figure 4d). On the other hand, CU Cu_2O/RGO 2:1 showed the highest *CO/products* ratio and confirmed the improved selectivity toward the formation of CO. The overall behaviors follow similar trends even at the other considered voltages. At −0.7 V vs. RHE, the activity of HER becomes predominant compared to CO_2RR, favored by the high concentration of protons in the aqueous-based electrolytes (Figure S8) [49,50]. Cu_2O/RGO 2:1 still shows the highest FE_{CO} (38%) compared to all the other materials: the selectivity towards HER is the lowest meaning that the synergistic effects of coupling between the two counterparts of the composite suppress the formation of H_2 and improved the activity of CO_2RR. This composition shows interesting properties in terms of selectivity and mostly productivity, with a ratio of CO compared to all the material that is almost double (0.39) respect to those obtained for other prepared composites, during the 120 min of experiment. The high faradaic efficiency at a relatively low applied voltage suggested an efficient formation of CO by the Cu_2O/RGO 2:1 composite, attesting improved selectivity compared to RGO-based systems reported in the literature (Table S3) [51–55]. At the most reductive voltage (−1.1 V vs. RHE), the high overvoltage relies on an improved selectivity of the different catalysts towards the CO_2RR process and higher productivities for ethylene, formic acid and targeted CO. The effects of the voltages on the selectivity for the different fractions between Cu_2O and RGO in the composite are highlighted in Figure 5. Cu_2O/RGO 1:1 and 1:2 showed a similar catalytic response, with an important fraction of H_2 produced and low selectivity towards CO_2RR products, even at more reductive voltages. This might be attributed to the intrinsic activity of RGO towards HER and the similar sizes of Cu_2O nanoparticles in the two composites, since this parameter is considered crucial for the different behavior of an electrocatalyst. The activity changes when the fraction of Cu_2O is higher than RGO, where an improved dispersion of Cu_2O nanoparticles is observed. In this case, the lowest dimensions of Cu_2O nanoparticles and the synergistic effects due to the coupling with RGO sheets allowed an improved activity of CO_2RR reaction, with the highest FE_{CO} at all the considered voltages.

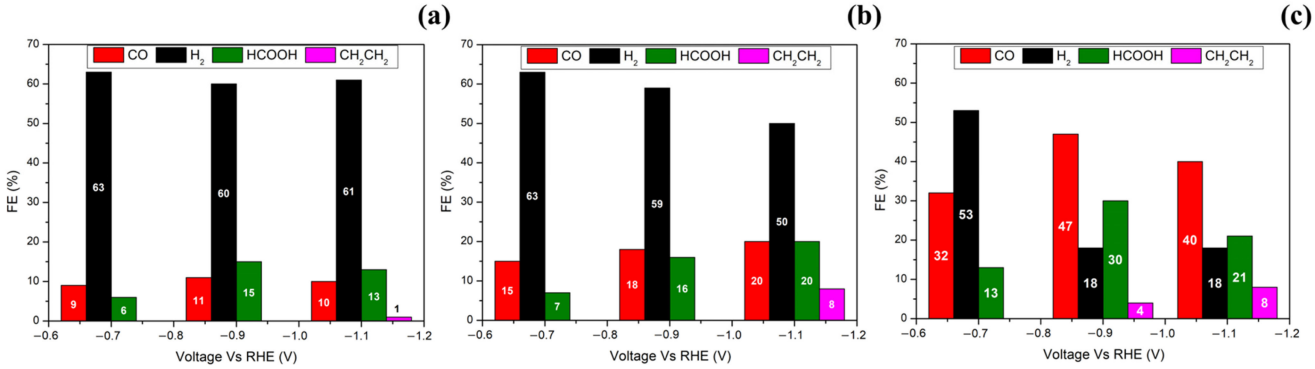

Figure 5. Faradaic efficiencies at the different voltages for the three composite CU Cu_2O/RGO. (**a**) CU Cu_2O/RGO 1:2, (**b**) CU Cu_2O/RGO 1:1 and (**c**) CU Cu_2O/RGO 2:1.

3. Materials and Methods

All reagents were pure and of analytical grade. Graphite, $NaNO_3$, H_2SO_4, $KMnO_4$ and H_2O_2 were utilized for the modified Hummer's method and the preparation of GO while, for the reduction of GO to RGO, NaOH and $H_2N_2{\cdot}2H_2O$ were used. SDS, $CuCl_2$, NH_2OH*HCl and NaOH were used as precursors for the synthesis of Cu_2O nanoparticles.

3.1. Preparation of the CU Cu_2O/RGO Composites

RGO was prepared via an adapted two-step method where graphite was initially converted to Graphene Oxide (GO) through a modified Hummer's method and reduced to obtain RGO [56,57]. In a typical procedure, 0.2 g of Graphite and 0.2 g of $NaNO_3$ were mixed in a round bottom flask with 10 mL of H_2SO_4 (95%). The solution was stirred at 400 rpm and kept in an ice bath for 30 min. Potassium Permanganate ($KMnO_4$, 1.2 g) was gradually added to the solution. After five minutes, 16 mL of Milli-Q H_2O was added, and the entire solution was stirred for one hour. GO is formed through addition of 40 mL of Milli-Q H_2O and 1.2 mL of H_2O_2 and stirring for one hour. The obtained powder of GO was washed with a 1:3 HCl solution to remove all the metal traces from the obtained material and with absolute ethanol; GO was then separated by filtration and dried. In the second step, GO was reduced to RGO by addition of a strong reducing agent such as $H_2N_2{\cdot}2H_2O$. In a typical procedure, 50 mg of GO was mixed with 50 mL of H_2O in a bottom flask. The pH of the mixture was corrected to 10–11 by the addition of 0.1 M NaOH solution and 4 mL of $H_2N_2{\cdot}2H_2O$ to start the reduction. The entire solution was stirred under reflux for one hour at 90 °C. RGO was filtrated under vacuum using a Millipore filter paper (pore size: 0.2 μm), washed with Milli-Q H_2O and absolute ethanol and dried at 50 °C for 12 h. All the composites were prepared via impregnation, growing Cu_2O nanoparticles on the support through an adapted method [58]. In particular, a proper amount of RGO (5, 10 and 20 mg, respectively, for the 2:1, 1:1 and 1:2 composites) was mixed with 0.348 g of SDS and 35.65 mL of Milli-Q H_2O and sonicated for 20 min at 30 °C. In total, 2 mL of a $CuCl_2$ 0.1 M solution were introduced dropwise under vigorous stirring and 0.72 mL of NaOH 1M and 1.6 mL of $NH_2OH{\cdot}HCl$ were added very quickly to the solution of $CuCl_2$, forming the Cu_2O nucleation seeds. The mixture was aged for 60 min at 30 °C, while the color of the solution changed from light blue to orange, confirming the formation of Cu_2O on the support. The materials were washed three times with absolute ethanol, separated from the solution by filtration and dried for 12 h at 45 °C in order to remove the surfactants from the surface of Cu_2O.

3.2. Characterization

The crystalline structure of the different materials was investigated by X-ray diffraction (XRD) using a high-resolution X-ray powder diffractometer (PANalytical X'Pert Pro MPD) with Cu Kα radiation (λ = 0.1541 nm). Raman spectra have been acquired using a Renishaw InVia™ confocal Raman microscope coupled with a 632 nm laser. The morphology of fabricated nanostructures was investigated using a TEM JEOL 2010 with a LaB_6 emission gun operating at 160 kV and a Hitachi FE-SEM 4800 SEM. EDX measurements had been performed using a Jeol-7900F SEM microscope with accelerating voltage of 5 kV. An Autolab PGSTAT 302N electrochemical workstation (Metrohm, The Netherlands) coupled with Nova softwarehad been used for all the electrochemical measurements. The analysis of the gaseous products (CO, CH_4, CH_2CH_2, CH_3CH_3) was performed using a J&W Select Permanent Gases/CO_2 column connected to a methanizer and a FID detector. The analysis of H_2 amount was performed using a Molsieve 5A plot column (Restek, 30m, 0.53 mm ID, 30 μm film) connected to a TCD detector. HCOOH accumulated in the liquid phase has been determined by ion chromatography using a Metrohm 833 instrument, mounting a column Metrosep A Supp 19-250/4.0 with eluent $NaHCO_3$ 1.0 mM/Na_2CO_3 3.2 mM.

3.3. Electrochemical Characterization

The Working Electrodes (WE) were prepared by drop casting 10 μL of an ink of the catalyst on a Rotating Disk Electrode (RDE), coupled with a graphite electrode as the Counter Electrode (CE) and a Saturated Calomel Electrode (SCE) as the Reference Electrode (RE). The ink was prepared dissolving 3.0 mg of catalyst in 1 mL of a 1:9 2-propanol:H_2O solution and 50 μL of Nafion. All the electrochemical characterization had been performed by rotating the RDE at 1600 RPM in a 0.1 M $KHCO_3$ solution. Linear Sweep Voltammetries

(LSV) had been performed by choosing a lower voltage limit and using a scan rate of 5 mV/s. The voltages were converted to RHE using the Equation (1)

$$V_{RHE} = V_{SCE} + 0.244\ V + 0.059 \times pH \quad (1)$$

Each LSV was repeated for three times to desorb all the gaseous species adsorbed on the surface of the electrode and to obtain a clear indication of the electrochemical behavior of the bare materials. All the experiments were carried out both in the Ar and CO_2 atmosphere, correcting the voltage with iR compensation. Even if the determination of the ECSA was performed to better characterize the electrochemical properties [59], it was decided to normalize the current measurements to the geometric area of the electrode due to the variability of the electrocatalysts deposition. Electrochemical Impedance Spectroscopy (EIS) analysis was performed at Open Circuit Voltage (OCV) in the frequency range of 100 kHz to 1 Hz. According to the literature [60], a Thin-Film (TF)–Rotating Disc Working Electrode (three–electrodes) cell setup was used to minimize the capacitance related to ionomer and carbon components.

3.4. CO_2RR Experiments

The WE was prepared by drop casting an ink of different catalyst powder on top of Toray carbon paper support. In a typical experiment, 3.0 mg of catalyst, 0.9 mL of milliQ H_2O, 0.1 mL of i-propanol and 50 µL of Nafion were mixed and sonicated for one hour. In total, 100 µL of solution was deposited on both sides of the carbon support, covering an area of 10 mm × 5 mm. The properly modified Toray paper support is used as WE in a gas-tight electrochemical cell, equipped with a platinum wire (1.00 mm as diameter, 99.9% of purity, Sigma Aldrich, St. Louis, MI, USA) as the CE and Ag/AgCl sat. electrode as the RE. The electrochemical characterization was performed purging 20 mL/min of CO_2 in 15 mL of $KHCO_3$ 0.1 M (purity > 99.95%, Sigma Aldrich). The different electrocatalyst materials were studied performing chronoamperometries for 120 min, analyzing the gaseous products through gas-chromatography and the liquid products by ionic chromatography by taking 1 mL of aliquot and replacing it with fresh electrolyte. A 5 cycle-CV with a scan rate of 100 mV/s was performed before each experiment in order to clean the surface of the catalyst from the adsorbed gaseous species. CAs had been studied at −1.3 V, −1.5 V and −1.7 V vs. Ag/AgCl, using the Equation (2) to convert the voltages to RHE.

$$V_{RHE} = V_{Ag/AgCl} + 0.197\ V + 0.059 \times pH \quad (2)$$

All the voltages were corrected for iR compensation and normalized for the geometrical area and each WE was substituted after each electrochemical characterization. The total Faradaic Efficiency (FE) was calculated from the final concentration of the different products during the time by Equation (3):

$$FE = \frac{n_e \times n \times F}{Q} \quad (3)$$

where n_e the number of electrons involved in the particular reductive reaction, n is the total moles of the product, F is the Faraday constant and Q is the total charge.

4. Conclusions

In summary, in this work we successfully prepared different composites of Cu_2O/RGO through a multistep approach where nanocubes of Cu_2O were grown on crumpled RGO nanosheets. The detailed characterization of the prepared materials provided valuable insights into the structural and morphological properties, observing the purity of the crystalline phase and the contemporaneous coexistence of Cu_2O and RGO in the composites. SEM and TEM images unveiled the morphology of the materials, revealing an intimate contact between the two counterparts of the material and the beneficial effects on size and distribution of Cu_2O nanoparticles. The electrocatalytic performance of the synthetized

materials was evaluated through a three-electrode setup highlighting the improved overall activity of the composites thanks to the enhanced dispersion of Cu_2O and the intimate contact with RGO sheets. CO_2RR experiments revealed an enhanced current density for the composites, especially at lower voltages, and improved faradaic efficiencies for the products of the reduction, in particular CO. The sample Cu_2O/RGO 2:1 showed a selective formation of CO over H_2, with a faradaic efficiency of 50% at −0.9 V vs. RHE and revealed the advantageous pathway towards the formation of *CO intermediate even at lower voltages. The increased current (−2.72 mA/cm^2 for CU Cu_2O/RGO 2:1, compared to −1.79 mA/cm^2 for Cu_2O at the voltage of −0.9 V vs. RHE and in the CO_2 atmosphere) and selectivity in this composition resulted in significantly higher amounts of produced CO, providing a valuable solution for the formation of effective interphases and the promotion of catalytic properties in nanostructured materials.

Supplementary Materials: The following supporting information can be downloaded at: https://www.mdpi.com/article/10.3390/catal14070412/s1, Figure S1: Rietveld analysis of the CU Cu_2O/RGO 2:1 diffractogram. Figure S2: Raman spectrum of pure RGO with the characteristics vibrations. Table S1: Weight fraction of the different CU Cu_2O/RGO materials from TGA analysis. Figure S3: SEM and TEM images of pristine RGO and CU Cu_2O. Figure S4: Size distribution for the different materials. Table S2: Size of Cu_2O nanoparticles on the different composites. Figure S5: LSVs at −0.6 V, −0.8 V and −1.0 V vs. RHE for the different materials. Figure S6: CAs at −0.6 V, −0.8 V and −1.0 V vs. RHE for the different materials. Figure S7: Nyquist plot at OCV of the different materials performed in CO_2 saturated atmosphere. Figure S8: CO_2RR tests for the different composites of CU Cu_2O/RGO at the voltage of −0.7 V vs. RHE. Figure S9: CO_2RR tests for the different composites of CU Cu_2O/RGO at the voltage of −1.1 V vs. RHE. Table S3: Comparison with literature. Table S4: ECSA obtained for the different materials. Refences.

Author Contributions: Conceptualization, M.B. (Matteo Bisetto), M.B. (Manuela Bevilacqua). and P.F.; methodology, M.B. (Matteo Bisetto), S.R., M.B. (Manuela Bevilacqua) and T.M.; validation, T.M. and A.N.; formal analysis, M.B. (Matteo Bisetto); investigation, M.B. (Matteo Bisetto) and S.R.; data curation, M.B. (Matteo Bisetto) and M.B. (Manuela Bevilacqua); writing—original draft preparation, M.B. (Matteo Bisetto) and M.B. (Manuela Bevilacqua); writing—review and editing, A.N., T.M. and P.F.; resources, A.N. and P.F.; supervision, P.F. All authors have read and agreed to the published version of the manuscript.

Funding: This research was funded by the European Community, (projects H2020–LC–SC3-2019-NZE-RES-CC), grant agreement number 884444. A.N. acknowledges the support from the Project CH4.0 under the MIUR program "Dipartimenti di Eccellenza 2023-2027" (CUP: D13C2200352001).

Data Availability Statement: The data that support the findings of this study are available from the corresponding author upon reasonable request.

Acknowledgments: We would like to thank Luca Mascaretti for the measurements at RCPTM, Giuliano Giambastiani for the TGA measurements and Elvio Merlac from the University of Trieste for the development of the electrochemical device.

Conflicts of Interest: The authors declare no conflicts of interest.

References

1. Khdary, N.H.; Alayyar, A.S.; Alsarhan, L.M.; Alshihri, S.; Mokhtar, M. Metal Oxides as Catalyst/Supporter for CO_2 Capture and Conversion, Review. *Catalysts* **2022**, *12*, 300. [CrossRef]
2. Xia, Q.; Zhang, K.; Zheng, T.; An, L.; Xia, C.; Zhang, X. Integration of CO_2 Capture and Electrochemical Conversion. *ACS Energy Lett.* **2023**, *8*, 2840–2857. [CrossRef]
3. He, Y.; Müller, F.H.; Palkovits, R.; Zeng, F.; Mebrahtu, C. Tandem Catalysis for CO_2 Conversion to Higher Alcohols: A Review. *Appl. Catal. B Environ.* **2024**, *345*, 123663. [CrossRef]
4. Ma, Y.; Wang, Z.; Xu, X.; Wang, J. Review on Porous Nanomaterials for Adsorption and Photocatalytic Conversion of CO_2. *Cuihua Xuebao/Chinese J. Catal.* **2017**, *38*, 1956–1969. [CrossRef]
5. Lee, Y.Y.; Jung, H.S.; Kim, J.M.; Kang, Y.T. Photocatalytic CO_2 Conversion on Highly Ordered Mesoporous Materials: Comparisons of Metal Oxides and Compound Semiconductors. *Appl. Catal. B Environ.* **2018**, *224*, 594–601. [CrossRef]
6. Christoforidis, K.C.; Fornasiero, P. Photocatalysis for Hydrogen Production and CO_2 Reduction: The Case of Copper-Catalysts. *ChemCatChem* **2019**, *11*, 368–382. [CrossRef]

7. Verma, R.; Belgamwar, R.; Polshettiwar, V. Plasmonic Photocatalysis for CO_2 Conversion to Chemicals and Fuels. *ACS Mater. Lett.* **2021**, *3*, 574–598. [CrossRef]
8. Rej, S.; Bisetto, M.; Naldoni, A.; Fornasiero, P. Well-Defined Cu_2O Photocatalysts for Solar Fuels and Chemicals. *J. Mater. Chem. A* **2021**, *9*, 5915–5951. [CrossRef]
9. Zhang, Y.; Huang, Y.; Zhu, S.S.; Liu, Y.Y.; Zhang, X.; Wang, J.J.; Braun, A. Covalent S-O Bonding Enables Enhanced Photoelectrochemical Performance of Cu_2S/Fe_2O_3 Heterojunction for Water Splitting. *Small* **2021**, *17*, 2100320. [CrossRef]
10. Ma, X.; Zhang, Y.; Fan, T.; Wei, D.; Huang, Z.; Zhang, Z.; Zhang, Z.; Dong, Y.; Hong, Q.; Chen, Z.; et al. Facet Dopant Regulation of Cu_2O Boosts Electrocatalytic CO_2 Reduction to Formate. *Adv. Funct. Mater.* **2023**, *33*, 2213145. [CrossRef]
11. Jun, M.; Kwak, C.; Lee, S.Y.; Joo, J.; Kim, J.M.; Im, D.J.; Cho, M.K.; Baik, H.; Hwang, Y.J.; Kim, H.; et al. Microfluidics-Assisted Synthesis of Hierarchical Cu_2O Nanocrystal as C_2-Selective CO_2 Reduction Electrocatalyst. *Small Methods* **2022**, *6*, 2200074. [CrossRef] [PubMed]
12. Ren, D.; Deng, Y.; Handoko, A.D.; Chen, C.S.; Malkhandi, S.; Yeo, B.S. Selective Electrochemical Reduction of Carbon Dioxide to Ethylene and Ethanol on Copper(I) Oxide Catalysts. *ACS Catal.* **2015**, *5*, 2814–2821. [CrossRef]
13. Mistry, H.; Varela, A.S.; Bonifacio, C.S.; Zegkinoglou, I.; Sinev, I.; Choi, Y.W.; Kisslinger, K.; Stach, E.A.; Yang, J.C.; Strasser, P.; et al. Highly Selective Plasma-Activated Copper Catalysts for Carbon Dioxide Reduction to Ethylene. *Nat. Commun.* **2016**, *7*, 12123. [CrossRef]
14. Wang, S.; Kou, T.; Baker, S.E.; Duoss, E.B.; Li, Y. Recent Progress in Electrochemical Reduction of CO_2 by Oxide-Derived Copper Catalysts. *Mater. Today Nano* **2020**, *12*, 100096. [CrossRef]
15. Liu, J.; Cheng, L.; Wang, Y.; Chen, R.; Xiao, C.; Zhou, X.; Zhu, Y.; Li, Y.; Li, C. Dynamic Determination of Cu^+ Roles for CO_2 Reduction on Electrochemically Stable Cu_2O-Based Nanocubes. *J. Mater. Chem. A* **2022**, *10*, 8459–8465. [CrossRef]
16. Jiang, Y.; Wang, X.; Duan, D.; He, C.; Ma, J.; Zhang, W.; Liu, H.; Long, R.; Li, Z.; Kong, T.; et al. Structural Reconstruction of Cu_2O Superparticles toward Electrocatalytic CO_2 Reduction with High C_{2+} Products Selectivity. *Adv. Sci.* **2022**, *9*, 2105292. [CrossRef]
17. Larrazábal, G.O.; Okatenko, V.; Chorkendorff, I.; Buonsanti, R.; Seger, B. Investigation of Ethylene and Propylene Production from CO_2 Reduction over Copper Nanocubes in an MEA-Type Electrolyzer. *ACS Appl. Mater. Interfaces* **2022**, *14*, 7779–7787. [CrossRef] [PubMed]
18. Guo, S.; Liu, Y.; Huang, Y.; Wang, H.; Murphy, E.; Delafontaine, L.; Chen, J.; Zenyuk, I.V.; Atanassov, P. Promoting Electrolysis of Carbon Monoxide toward Acetate and 1-Propanol in Flow Electrolyzer. *ACS Energy Lett.* **2023**, *8*, 935–942. [CrossRef]
19. Wu, Q.; Du, R.; Wang, P.; Waterhouse, G.I.N.; Li, J.; Qiu, Y.; Yan, K.; Zhao, Y.; Zhao, W.W.; Tsai, H.J.; et al. Nanograin-Boundary-Abundant Cu_2O-Cu Nanocubes with High C_{2+} Selectivity and Good Stability during Electrochemical CO_2 Reduction at a Current Density of 500 mA/cm^2. *ACS Nano* **2023**, *17*, 12884–12894. [CrossRef]
20. Zaza, L.; Rossi, K.; Buonsanti, R. Well-Defined Copper-Based Nanocatalysts for Selective Electrochemical Reduction of CO_2 to C_2 Products. *ACS Energy Lett.* **2022**, *7*, 1284–1291. [CrossRef]
21. Rossi, K.; Buonsanti, R. Shaping Copper Nanocatalysts to Steer Selectivity in the Electrochemical CO_2 Reduction Reaction. *Acc. Chem. Res.* **2022**, *55*, 629–637. [CrossRef] [PubMed]
22. Liu, L.; Corma, A. Metal Catalysts for Heterogeneous Catalysis: From Single Atoms to Nanoclusters and Nanoparticles. *Chem. Rev.* **2018**, *118*, 4981–5079. [CrossRef] [PubMed]
23. Zhai, Z.; Guo, X.; Jiao, Z.; Jin, G.; Guo, X.Y. Graphene-Supported Cu_2O Nanoparticles: An Efficient Heterogeneous Catalyst for C-O Cross-Coupling of Aryl Iodides with Phenols. *Catal. Sci. Technol.* **2014**, *4*, 4196–4199. [CrossRef]
24. Abu-Zied, B.M.; Hussein, M.A.; Khan, A.; Asiri, A.M. Cu-Cu_2O@graphene Nanoplatelets Nanocomposites: Facile Synthesis, Characterization, and Electrical Conductivity Properties. *Mater. Chem. Phys.* **2018**, *213*, 168–176. [CrossRef]
25. Alhaddad, M.; Navarro, R.M.; Hussein, M.A.; Mohamed, R.M. Visible Light Production of Hydrogen from Glycerol over Cu_2O-gC_3N_4 Nanocomposites with Enhanced Photocatalytic Efficiency. *J. Mater. Res. Technol.* **2020**, *9*, 15335–15345. [CrossRef]
26. Wu, Z.; Wang, C.; Zhang, X.; Guo, Q.; Wang, J. Graphene-Based CO_2 Reduction Electrocatalysts: A Review. *New Carbon Mater.* **2024**, *39*, 100–130. [CrossRef]
27. Zhang, D.; Wei, D.; Cui, Z.; Wang, S.; Yang, S.; Cao, M.; Hu, C. Improving Water Splitting Performance of Cu_2O through a Synergistic "Two-Way Transfer" Process of Cu and Graphene. *Phys. Chem. Chem. Phys.* **2014**, *16*, 25531–25536. [CrossRef] [PubMed]
28. Nemiwal, M.; Zhang, T.C.; Kumar, D. Graphene-Based Electrocatalysts: Hydrogen Evolution Reactions and Overall Water Splitting. *Int. J. Hydrogen Energy* **2021**, *46*, 21401–21418. [CrossRef]
29. Sharma, V.; Jain, Y.; Kumari, M.; Gupta, R.; Sharma, S.K.; Sachdev, K. Synthesis and Characterization of Graphene Oxide (GO) and Reduced Graphene Oxide (RGO) for Gas Sensing Application. *Macromol. Symp.* **2017**, *376*, 1700006. [CrossRef]
30. Yoon, Y.; Kye, H.; Yang, W.S.; Kang, J.W. Comparing Graphene Oxide and Reduced Graphene Oxide as Blending Materials for Polysulfone and Polyvinylidene Difluoride Membranes. *Appl. Sci.* **2020**, *10*, 2015. [CrossRef]
31. Jaafar, E.; Kashif, M.; Sahari, S.K.; Ngaini, Z. Study on Morphological, Optical and Electrical Properties of Graphene Oxide (GO) and Reduced Graphene Oxide (RGO). *Mater. Sci. Forum* **2018**, *917*, 112–116. [CrossRef]
32. Wang, W.; Ning, H.; Yang, Z.; Feng, Z.; Wang, J.; Wang, X.; Mao, Q.; Wu, W.; Zhao, Q.; Hu, H.; et al. Interface-Induced Controllable Synthesis of Cu_2O Nanocubes for Electroreduction CO_2 to C_2H_4. *Electrochim. Acta* **2019**, *306*, 360–365. [CrossRef]
33. Susman, M.D.; Feldman, Y.; Vaskevich, A.; Rubinstein, I. Chemical Deposition of Cu_2O Nanocrystals with Precise Morphology Control. *ACS Nano* **2014**, *8*, 162–174. [CrossRef] [PubMed]

34. An, X.; Li, K.; Tang, J. Cu_2O/Reduced Graphene Oxide Composites for the Photocatalytic Conversion of CO_2. *ChemSusChem* **2014**, *7*, 1086–1093. [CrossRef] [PubMed]
35. Fu, W.; Liu, Z.; Wang, T.; Liang, J.; Duan, S.; Xie, L.; Han, J.; Li, Q. Promoting C_{2+} Production from Electrochemical CO_2 Reduction on Shape-Controlled Cuprous Oxide Nanocrystals with High-Index Facets. *ACS Sustain. Chem. Eng.* **2020**, *8*, 15223–15229. [CrossRef]
36. Xu, J.; Wang, R.; Chen, X.; Zhou, R.; Zhang, J. Cu_2SnS_3 Nanocrystals Decorated RGO Nanosheets towards Efficient and Stable Hydrogen Evolution Reaction in Both Acid and Alkaline Solutions. *Mater. Today Energy* **2020**, *17*, 100435. [CrossRef]
37. Khanra, P.; Kuila, T.; Kim, N.H.; Bae, S.H.; Yu, D.-S.; Lee, J.H. Simultaneous Bio-Functionalization and Reduction of Graphene Oxide by Baker's Yeast. *Chem. Eng. J.* **2012**, *183*, 526–533. [CrossRef]
38. Sadhukhan, S.; Ghosh, T.K.; Rana, D.; Roy, I.; Bhattacharyya, A.; Sarkar, G.; Chakraborty, M.; Chattopadhyay, D. Studies on Synthesis of Reduced Graphene Oxide (RGO) via Green Route and Its Electrical Property. *Mater. Res. Bull.* **2016**, *79*, 41–51. [CrossRef]
39. Wang, Y.; Shi, Z.X.; Yin, J. Facile Synthesis of Soluble Graphene via a Green Reduction of Graphene Oxide in Tea Solution and Its Biocomposites. *ACS Appl. Mater. Interfaces* **2011**, *3*, 1127–1133. [CrossRef]
40. Cui, P.; Lee, J.; Hwang, E.; Lee, H. One-Pot Reduction of Graphene Oxide at Subzero Temperatures. *Chem. Commun.* **2011**, *47*, 12370–12372. [CrossRef]
41. Kuila, T.; Mishra, A.K.; Khanra, P.; Kim, N.H.; Lee, J.H. Recent Advances in the Efficient Reduction of Graphene Oxide and Its Application as Energy Storage Electrode Materials. *Nanoscale* **2013**, *5*, 52–71. [CrossRef] [PubMed]
42. Gao, L.; Pang, C.; He, D.; Shen, L.; Gupta, A.; Bao, N. Synthesis of Hierarchical Nanoporous Microstructures via the Kirkendall Effect in Chemical Reduction Process. *Sci. Rep.* **2015**, *5*, 16061. [CrossRef] [PubMed]
43. Möller, T.; Scholten, F.; Thanh, T.N.; Sinev, I.; Timoshenko, J.; Wang, X.; Jovanov, Z.; Gliech, M.; Roldan Cuenya, B.; Varela, A.S.; et al. Electrocatalytic CO_2 Reduction on CuO_x Nanocubes: Tracking the Evolution of Chemical State, Geometric Structure, and Catalytic Selectivity Using Operando Spectroscopy. *Angew. Chemie Int. Ed.* **2020**, *59*, 17974–17983. [CrossRef] [PubMed]
44. Nallal, M.; Park, K.H.; Park, S.; Kim, J.; Shenoy, S.; Chuaicham, C.; Sasaki, K.; Sekar, K. Cu_2O/Reduced Graphene Oxide Nanocomposites for Electrocatalytic Overall Water Splitting. *ACS Appl. Nano Mater.* **2022**, *5*, 17271–17280. [CrossRef]
45. Zhong, Y.; Wang, S.; Li, M.; Ma, J.; Song, S.; Kumar, A.; Duan, H.; Kuang, Y.; Sun, X. Rational Design of Copper-Based Electrocatalysts and Electrochemical Systems for CO_2 Reduction: From Active Sites Engineering to Mass Transfer Dynamics. *Mater. Today Phys.* **2021**, *18*, 100354. [CrossRef]
46. Dattila, F.; Garclá-Muelas, R.; López, N. Active and Selective Ensembles in Oxide-Derived Copper Catalysts for CO_2 Reduction. *ACS Energy Lett.* **2020**, *5*, 3176–3184. [CrossRef]
47. Cao, X.; Cao, G.; Li, M.; Zhu, X.; Han, J.; Ge, Q.; Wang, H. Enhanced Ethylene Formation from Carbon Dioxide Reduction through Sequential Catalysis on Au Decorated Cubic Cu_2O Electrocatalyst. *Eur. J. Inorg. Chem.* **2021**, *2021*, 2353–2364. [CrossRef]
48. Zheng, T.; Liu, C.; Guo, C.; Zhang, M.; Li, X.; Jiang, Q.; Xue, W.; Li, H.; Li, A.; Pao, C.W.; et al. Copper-Catalysed Exclusive CO_2 to Pure Formic Acid Conversion via Single-Atom Alloying. *Nat. Nanotechnol.* **2021**, *16*, 1386–1393. [CrossRef] [PubMed]
49. Lee, C.W.; Kim, C.; Min, B.K. Theoretical Insights into Selective Electrochemical Conversion of Carbon Dioxide. *Nano Converg.* **2019**, *6*, 8. [CrossRef]
50. Goyal, A.; Marcandalli, G.; Mints, V.A.; Koper, M.T.M. Competition between CO_2 Reduction and Hydrogen Evolution on a Gold Electrode under Well-Defined Mass Transport Conditions. *J. Am. Chem. Soc.* **2020**, *142*, 4154–4161. [CrossRef]
51. Cao, C.; Wen, Z. Cu Nanoparticles Decorating RGO Nanohybrids as Electrocatalyst toward CO_2 Reduction. *J. CO2 Util.* **2017**, *22*, 231–237. [CrossRef]
52. Ning, H.; Mao, Q.; Wang, W.; Yang, Z.; Wang, X.; Zhao, Q.; Song, Y.; Wu, M. N-Doped Reduced Graphene Oxide Supported Cu_2O Nanocubes as High Active Catalyst for CO_2 Electroreduction to C_2H_4. *J. Alloys Compd.* **2019**, *785*, 7–12. [CrossRef]
53. Bochlin, Y.; Korin, E.; Bettelheim, A. Different Pathways for CO_2 Electrocatalytic Reduction by Confined CoTMPyP in Electrodeposited Reduced Graphene Oxide. *ACS Appl. Energy Mater.* **2019**, *2*, 8434–8440. [CrossRef]
54. Nguyen, D.L.T.; Lee, C.W.; Na, J.; Kim, M.C.; Tu, N.D.K.; Lee, S.Y.; Sa, Y.J.; Won, D.H.; Oh, H.S.; Kim, H.; et al. Mass Transport Control by Surface Graphene Oxide for Selective CO Production from Electrochemical CO_2 Reduction. *ACS Catal.* **2020**, *10*, 3222–3231. [CrossRef]
55. Jiang, X.; Wang, Q.; Xiao, X.; Chen, J.; Shen, Y.; Wang, M. Interfacial Engineering of Bismuth with Reduced Graphene Oxide Hybrid for Improving CO_2 Electroreduction Performance. *Electrochim. Acta* **2020**, *357*, 136840. [CrossRef]
56. Ramakrishnan, M.C.; Thangavelu, R.R. Synthesis and Characterization of Reduced Graphene Oxide. *Adv. Mater. Res.* **2013**, *678*, 56–60. [CrossRef]
57. Bansal, K.; Singh, J.; Dhaliwal, A.S. Synthesis and Characterization of Graphene Oxide and Its Reduction with Different Reducing Agents. *IOP Conf. Ser. Mater. Sci. Eng.* **2022**, *1225*, 012050. [CrossRef]
58. Chanda, K.; Rej, S.; Huang, M.H. Investigation of Facet Effects on the Catalytic Activity of Cu_2O Nanocrystals for Efficient Regioselective Synthesis of 3,5-Disubstituted Isoxazoles. *Nanoscale* **2013**, *5*, 12494–12501. [CrossRef]

59. Zhuang, T.T.; Liang, Z.Q.; Seifitokaldani, A.; Li, Y.; De Luna, P.; Burdyny, T.; Che, F.; Meng, F.; Min, Y.; Quintero-Bermudez, R.; et al. Steering Post-C-C Coupling Selectivity Enables High Efficiency Electroreduction of Carbon Dioxide to Multi-Carbon Alcohols. *Nat. Catal.* **2018**, *1*, 421–428. [CrossRef]
60. Singh, R.K.; Devivaraprasad, R.; Kar, T.; Chakraborty, A.; Neergat, M. Electrochemical Impedance Spectroscopy of Oxygen Reduction Reaction (ORR) in a Rotating Disk Electrode Configuration: Effect of Ionomer Content and Carbon-Support. *J. Electrochem. Soc.* **2015**, *162*, F489–F498. [CrossRef]